Langmuir

ARTICLE

pubs.acs.org/Langmuir

Self-Assembled Monolayers Derived from Alkoxyphenylethanethiols Having One, Two, and Three Pendant Chains

Supachai Rittikulsittichai, Andrew C. Jamison, and T. Randall Lee*

Department of Chemistry and the Texas Center for Superconductivity, University of Houston, Houston, Texas 77204-5003, United States

Supporting Information

ABSTRACT: This article describes the design, synthesis, and study of alkoxyphenylethanethiol-based adsorbates with one (**R1ArMT**), two (**R2ArMT**), and three (**R3ArMT**) pendant octadecyloxy chains substituted at the 4-, 3,5-, and 3,4,5-positions, respectively, of the phenylethanethiol group. These adsorbates are being developed for use in the preparation of compositionally versatile "mixed" self-assembled monolayer (SAM) coatings. The resultant SAMs were characterized by ellipsometry, contact angle goniometry, polarization modulation infrared reflection−absorption spectroscopy (PM-IRRAS), and X-ray photoelectron spectroscopy (XPS). The studies revealed that **R1ArMT** generates a well-ordered monolayer film, while **R2ArMT** and **R3ArMT** generate monolayer films with diminished conformational order in which the degree of crystallinity decreases as follows: **C18** ∼ **R1ArMT** > **R3ArMT** > **R2ArMT**. In addition, comparison of the molecular and chain packing densities of SAMs derived from these new adsorbates reveals that the **R2ArMT** and **R3ArMT** adsorbates give rise to SAMs with reduced chain tilt and smaller surface area per chain when compared to the SAMs derived from **C18** and **R1ArMT**.

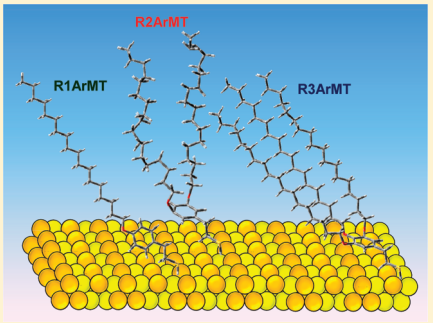

INTRODUCTION

Self-assembled monolayers (SAMs) derived from the adsorption of alkanethiols on gold have found widespread use in microelectronic,[1−3] biomedical,[4−6] micromechanical,[7−10] and catalytic[11] applications. The successful implementation of SAMs in many of these applications requires an understanding of their surface orientation, packing structure, and interfacial properties. These features are governed at a fundamental level by molecule−molecule and molecule−substrate interactions.[12−19] Accordingly, a number of structurally unique adsorbates having a variety of headgroups,[20−23] spacers,[9,24−30] and tailgroups have been designed, fabricated, and studied. Researchers have found, for example, that the incorporation of an aromatic moiety within a long alkanethiol chain can influence the packing of the molecular assembly; even a simple phenyl ring can break the cylindrical symmetry of an alkyl chain and introduce a kink along the chain.[31−34] Evans et al. examined the influence of the position of a phenylsulfonyl group along the backbone of hexadecanethiol (**C16**)[33] and found that the aromatic ring separated the hydrocarbon chain into two distinct portions: above and below the aromatic group. Adsorbates having a lengthy alkyl chain above the aromatic ring exhibited a faster rate of film formation, a more ordered conformational arrangement, and a higher packing density than those having a lengthy alkyl chain below the aromatic ring. These results therefore offer some rudimentary guidelines for the design of aromatic-containing alkanethiolate SAMs.

For adsorbates that possess structurally distinct molecular components, the commensurability of these layers within the monolayer film must be considered. As a specific example, a rigid planar aromatic system coupled to a long alkyl chain creates a surface structure in which the size match of the cross-sectional areas (S_m) of the different molecular parts must be considered for optimizing the packing and order of the resultant film.[15,16,18,31−34] More specifically, a sterically large headgroup requires a large lateral area on a substrate; consequently, the alkyl chains above an aromatic headgroup might tilt substantially to optimize the van der Waals interactions.

Other important factors that can influence the structural orientation and packing of monolayer films are the lattice binding sites and the binding geometry of the headgroups on the substrate.[15−19] For example, Tao and co-workers investigated the impact of thiolate binding geometry and aromatic bulk on the packing density and orientation of terminal hydrocarbon chains. These studies compared the adsorption of 4′-alkoxybiphenyl-4-methanethiol, (6-alkoxynaphth-2-yl)methanethiol, and 4′-alkoxybiphenylthiol on Au and Ag substrates.[18] The results suggested that the binding geometry of sulfur can adopt either sp^3 or sp hybridization, depending on the packing interaction of the aromatic rings.[18] All headgroups for these adsorbates occupied the same lattice positions on Au and Ag substrates, demonstrating that adsorbates with aromatic headgroups of different size can still be commensurate with the $(\sqrt{3} \times \sqrt{3})R30°$ lattice that is characteristic of well-ordered normal alkanethiolate SAMs.[18,31,33,34] In contrast, if there is a mismatch between two parts of an adsorbate

Received: April 11, 2011
Revised: May 30, 2011
Published: July 12, 2011

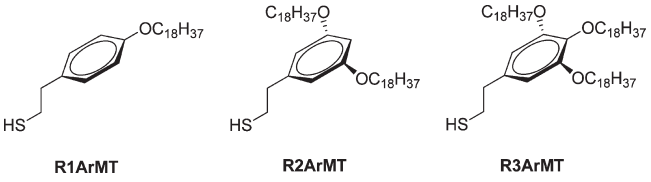

Figure 1. Structures of alkoxyphenylethanethiols having one (**R1ArMT**), two (**R2ArMT**), and three (**R3ArMT**) tailgroups.

or the binding sites of the headgroups are not appropriate for the development of a well-organized SAM, the molecular assemblies may adopt disordered or more liquidlike structures.[31,33,34]

Although the aforementioned studies (and others in which the aromatic moieties are positioned at the chain terminus)[9,16,18,31−33] have focused on adsorbates with single-chain tailgroups, there has been no systematic study of aromatic-containing adsorbates with multiple tailgroups, despite the fact that these adsorbates have the potential to tune the packing density of SAMs and to generate multicomponent interfaces simply by assigning distinct chemical signatures to the tailgroups within a judiciously designed adsorbate. To this end, the present study examines SAMs on gold derived from a series of new alkoxyphenylethanethiols that possess chain-to-headgroup ratios varying systematically from 1:1 to 3:1 (see **R1ArMT**, **R2ArMT**, and **R3ArMT** in Figure 1). We targeted adsorbates with long alkoxy chains, $CH_3(CH_2)_{18}O-Ar$, rather than short chains because we wished to generate and study SAMs with sufficient conformational order to detect systematic changes in their structure and interfacial properties.[14,30,35,36] Studies of such SAMs will advance our understanding of the factors that govern structurally complex monolayer interfaces and allow us to generate and study model interfaces that mimic the complexity found in nature (e.g., cell surfaces) and in advanced applied materials (e.g., heterogeneous polymer coatings).

EXPERIMENTAL SECTION

Adsorbate Synthesis. Detailed procedures for the synthesis of **R1ArMT**, **R2ArMT**, and **R3ArMT** are provided as Supporting Information. The respective starting materials, methyl 4-hydroxyphenylacetate, methyl 3,5-dihydroxyphenylacetate, and methyl 3,4,5-trihydroxy benzoate, were commercially available from Aldrich.

Preparation of SAMs. Ethanolic solutions of all adsorbates were prepared at 1 mM concentration in 25 mL glass vials, which were previously cleaned with piranha solution (3:1 mixture of H_2SO_4/30% H_2O_2) and rinsed thoroughly with deionized water and then absolute ethanol before use. [*Caution: piranha solution is highly corrosive, should never be stored, and should be handled with extreme care.*] A thin layer of gold (1000 Å) was evaporated on chromium-primed (100 Å Cr) Si(100) wafers, which were then cut into slides (1 × 4 cm) and cleaned by rinsing with absolute ethanol and drying under a flow of ultrapure nitrogen. These gold substrates were immersed in the adsorbate solutions and allowed to equilibrate for a period of 72 h. The resulting SAMs were thoroughly rinsed with toluene, THF, and ethanol and then blown dry with ultrapure nitrogen before characterization.

Ellipsometric Measurements. A Rudolf Research Auto EL III ellipsometer equipped with a He−Ne laser at a single wavelength of 632.8 nm at an angle of incidence of 70° was employed to measure the thicknesses of the SAMs. The optical constants of the gold substrates were obtained immediately after evaporation of the gold. To calculate the thicknesses of the SAMs, a refractive index of 1.45 was assumed for all measurements. Thickness values were collected and averaged for at least six measurements obtained from two separate slides using at least three different spots for each slide.

Table 1. Estimated Thicknesses and Measured Thicknesses for SAMs Generated from C18, R1ArMT, R2ArMT, and R3ArMT

adsorbate	estimated thickness (Å)	ellipsometric thickness (Å)[a]
C18	22	22
R1ArMT	27	28
R2ArMT	27	29
R3ArMT	27	29

[a] The ellipsometric thicknesses were reproducible within ±2 Å.

X-ray Photoelectron Spectroscopy (XPS). The composition and coverage of the monolayer films were measured with a PHI 5700 X-ray photoelectron spectrometer equipped with a monochromatic Al Kα X-ray source with a PHI 04091 neutralizer. The incident beam was positioned at 90° relative to the axis of a hemispherical energy analyzer with a photoelectron takeoff angle of 45° from the surface. The binding energies were referenced by setting the Au $4f_{7/2}$ peak at 84.0 eV.

Contact Angle Measurements. Contact angles were measured with a Ramé-Hart model 100 goniometer using water (H_2O), hexadecane (HD), and decalin (DEC). The contacting liquids were dispensed (advancing angle, θ_a) and withdrawn (receding angle, θ_r) on the surfaces of the SAMs using a Matrix Technologies micro-Electrapette 25 at the slowest possible speed (1 μL/s). The measurements were performed at room temperature (ca. 293 K) while keeping the pipet tip in contact with the drop. Reported values for each sample were the average of both drop edges taken from at least six independent drops of the contacting liquids from two separate slides.

Polarization Modulation Infrared Reflection−Absorption Spectroscopy (PM-IRRAS). The reflection−absorption spectra were recorded on a Nicolet NEXUS-IR 670 Fourier transform spectrometer equipped with a liquid nitrogen-cooled mercury−cadmium−telluride (MCT) detector and a Hinds Instruments PEM-90 photoelastic modulator operating at 37 Hz. The measurement chamber was maintained with a continuous flow of nitrogen gas during the course of the experiments. The spectra were collected at 2 cm^{-1} spectral resolution for 512 scans with a grazing angle for the infrared beam aligned at 80°.

RESULTS AND DISCUSSION

Ellipsometric Thicknesses. To provide a baseline comparison for the new adsorbates, we generated SAMs in parallel from octadecanethiol (**C18**). The ellipsometric measurements for all SAMs were all determined using a refractive index of $n = 1.45$, a value commonly assumed for similar organic thin films on gold.[23,37,38] The ellipsometric thickness measurements for **C18** and the new adsorbates are shown in Table 1. To assess the probable relationship between the film thicknesses and the orientations of the adsorbates on the SAMs generated from alkoxyphenylethanethiols, we constructed cartoons of these adsorbates using Gaussview software (see Figure 2).[39]

For these new adsorbates, the insertion of the phenyl ring between the ethanethiol headgroup and the extended alkoxy chains can perturb the structure of the corresponding monolayer films. A previous study found that the axis through the C1−C4 carbons of a phenyl ring positioned at the terminal position of an extended alkyl chain possessing an even number of methylene units tilts from the surface normal by ∼60°.[9] To conduct our analysis of the ellipsometric data, we assumed that the long alkoxy chains are all fully trans-extended above the intervening

dx.doi.org/10.1021/la201313g |*Langmuir* 2011, 27, 9920–9927

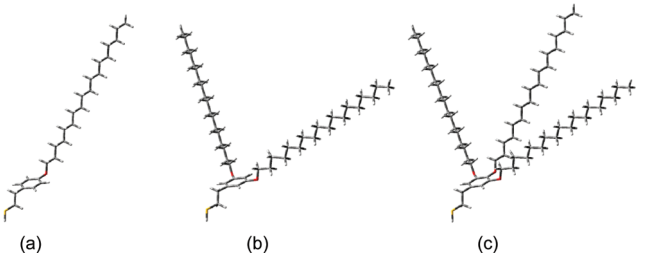

Figure 2. Structural representations of (a) **R1ArMT**, (b) **R2ArMT**, and (c) **R3ArMT**.

oxygen and tilted approximately 30° from the surface normal, in accord with that generally found with normal alkanethiolate SAMs on gold.[36] Additionally, the thickness of the **C18** reference film is known to be ~22 Å, and the thickness of alkanethiolate films on gold is known to increase ~1.3 Å with each incremental increase in the number of methylene units.[36] Given these assumptions and assuming a dense packing for the structures shown in Figure 2, we derived a rough estimate of the film thicknesses for each of our SAMs.[40]

For **R1ArMT**, the known thickness of the **C18** film thickness plus ~1.3 Å per each additional methylene unit gave an estimated film thickness of 22 + 2(1.3) = 24.6 Å for the alkyl chain segments. The estimated length of the C1−C4 axis along with the aromatic C−O bond distance is approximately 2.8 + 1.4 = 4.2 Å.[34] Assuming the phenoxy ring tilts ~60° from the surface normal, the thickness contribution of the phenoxy ring when the alkoxy chain is para to the ethanethiol linkage is calculated to be 4.2(cos 60°) + 1.5(cos 60°) = 2.85 Å, where the latter addend corresponds to the aliphatic C−O bond. Taken together, these values give an estimated thickness of ~27.4 Å for the SAM derived from **R1ArMT**. Similarly, for **R2ArMT**, the length of the C1−C3 axis of the phenyl ring can be estimated to be 2.8(cos 60°) + 1.5(cos 60°) = 2.65 Å, giving an estimated thickness of ~27.2 Å for the SAM derived from **R2ArMT**. For **R3ArMT**, given that there are two alkoxy chains meta and one para with respect to the headgroup, we can predict that the thickness will fall within the range of 27 Å.

Comparison of the estimated thicknesses with the measured thicknesses (see Table 1) reveals good agreement for the SAM derived from **R1ArMT**, but a slight underestimation for the SAMs derived from **R2ArMT** and **R3ArMT**. These results can be interpreted to indicate that the molecules of the **R1ArMT** SAMs tilt ~30° from the surface normal with the chains possessing a largely trans zigzag conformation. On the other hand, the underestimated thicknesses for the **R2ArMT** and **R3ArMT** SAMs can be interpreted to indicate that the molecules actually tilt less than 30° and/or that the molecules pack more densely on the surface than those in normal SAMs.

XPS Studies. Analysis of SAMs by XPS provides insight into their chemical composition, packing density, and headgroup−substrate interaction.[14,36,41,42] The quantitative packing density of SAMs can be determined from the atomic ratio of sulfur to gold (S/Au).[22] For SAMs having long alkyl chains, the sulfur signal is typically weak due to the low photoionization cross section and inelastic scattering attenuation of the S (2p) electrons by the overlying molecular structures.[43] In the present study, we have carefully analyzed the sulfur 2p peaks to quantify the atomic concentration of bound thiolate species on the gold surface. To afford a precise determination of S/Au ratio, we

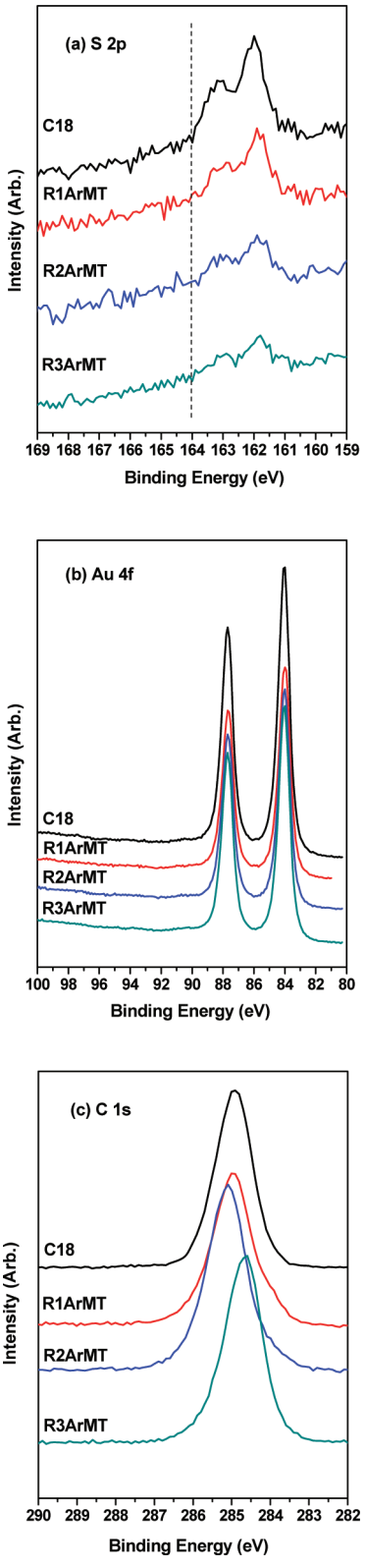

Figure 3. XPS spectra of the (a) S 2p, (b) Au 4f, and (c) C 1s regions of the monolayers derived from **C18**, **R1ArMT**, **R2ArMT**, and **R3ArMT**.

acquired high-resolution spectra of the core levels of sulfur and gold for all of the samples (Figures 3a and 3b, respectively). The peak positions for the S 2p region in Figure 3a reveal that SAMs

dx.doi.org/10.1021/la201313g |*Langmuir* 2011, 27, 9920–9927

Table 2. XPS Data for SAMs Derived from C18, R1ArMT, R2ArMT, and R3ArMT Used To Calculate the Relative Molecular Packing Densities

	integrated XPS peak area			
adsorbate	Au 4f	S 2p	S/Au	relative molecular packing density (%)
C18	94.61	5.39	0.059	100
R1ArMT	95.38	4.62	0.048	81
R2ArMT	96.12	3.88	0.040	68
R3ArMT	97.45	2.55	0.026	44

generated from the new class of adsorbates possess a binding energy of ca. 162−163.2 eV, indicating the presence of bound sulfur atoms on gold.[43,44] Peaks at ca. 164−166 and ∼169 eV, representing the binding energy of unbound sulfur[44] and oxidized forms of sulfur,[45] were not detected. These results demonstrate that the sulfur atoms of all of the new adsorbates bind to the surface of gold without oxidation during the course of preparation, development, or analysis.

Table 2 shows the quantitative packing densities of the **C18**, **R1ArMT**, **R2ArMT**, and **R3ArMT** SAMs determined from the S/Au ratios, which were 100%, 81%, 68%, and 44%, respectively, based on a normalized packing density for the **C18** SAM. The observed decrease in packing density of the aromatic-based monolayer films can be attributed, in part, to the steric bulk of the aromatic ring and an increase in the alkoxy chain-to-sulfur ratio. In the case of **R1ArMT**, the chain-to-headgroup ratio is 1:1, the same as **C18**, although the structural ordering of the **R1ArMT** SAM can plausibly be perturbed by the presence of the aromatic ring. The influence of the relatively large benzene moieties (21.8−25.2 Å^2 depending on orientation)[34] compared to the alkyl chain (18.4 Å^2)[34] gives rise to only a minor disruption in the packing of the chains compared to the **C18** film. The mismatch of cross-sectional areas between the phenyl ring adlayer and the long alkyl chain is estimated to be 10−25%.[34] Therefore, the introduction of a phenyl ring in the SAM film can lead to an increase of 10−25% in void space for the overlying alkyl chains. This model is consistent with the XPS-measured ∼19% reduction in packing density for the **R1ArMT** SAM.

The XPS data further indicate that by increasing the chain-to-headgroup ratio to 2:1 and 3:1 for **R2ArMT** and **R3ArMT**, respectively, there is both a decrease in the *molecular* packing density and an increase in the *tailgroup* density (136% and 132%, respectively, for the latter). On the basis of the measured packing density of the tailgroups and assuming that the alkyl chains are fully trans-extended, we can estimate the maximum possible tilt of the alkyl chains in these SAMs to be 36°, 23°, and 24° for the **R1ArMT**, **R2ArMT**, and **R3ArMT** SAMs, respectively. This analysis suggests that the average tilt of the chains in these SAMs is distinct for each of the adsorbates examined and further distinct from the 30° chain tilt of normal alkanethiolate SAMs on gold. Furthermore, the nature and magnitude of the tailgroup packing densities can influence both the assembly processes and the resultant structural quality of the films,[31−34] which will be discussed in the following sections.

Separately, the binding energy of C 1s can be used to estimate the packing density of the alkyl tailgroups in SAMs on gold.[22,46] It has been reported, for example, that the binding energy of the C 1s photoelectron for SAMs derived from *n*-alkanethiols shifts to a lower value when the alkyl chains are loosely packed.[41,42] This shift has been attributed to the fact that a loosely packed SAM acts as a poor insulator.[42] Consequently, the positive charges generated by photoelectron emission can be easily discharged. The XPS data in Figure 3c show broad symmetric C 1s peaks for all three adsorbates; the broadening of the peaks can be attributed to the overlap of the individual peaks for the binding energy of the methylene carbons and the carbon atoms of the benzene ring.[47] The C 1s peaks for the **C18** and **R1ArMT** SAMs appear at similar binding energies (±0.05 eV), while that of the **R2ArMT** SAM is shifted to slightly higher binding energy and that of the **R3ArMT** SAM is shifted to markedly lower binding energy. Based on these data, the relative alkyl chain packing density for the SAMs can be qualitatively approximated as follows: **R2ArMT** > **C18** ∼ **R1ArMT** ≫ **R3ArMT**. This trend is consistent with that obtained from the S/Au ratios (and the PM-IRRAS data; vide infra), save for the **R3ArMT** adsorbate.

It is noteworthy that the previous correlations between packing density and C 1s binding energy were derived from SAMs in which the adsorbates possessed relatively simple structures (e.g., *n*-alkanethiols or closely related species).[22,42,43,48,49] In these cases, the molecules (but not necessarily the tailgroups) pack densely on the surface with a relatively high S:Au ratio, and a shift of the C 1s binding energy to a lower value can be interpreted to indicate a SAM having loosely packed tailgroups that provide a reduced capacity for electronic insulation. In the case of **R3ArMT**, however, the tailgroups are densely packed, but the molecules (and specifically their sterically demanding headgroups) are loosely packed with a relatively low S:Au ratio. In this case, it is plausible that the loose packing near the headgroups and/or their sterically demanding geometry give(s) rise to pinhole-type defects that weaken the insulating capacity of the **R3ArMT** films despite their having densely packed tailgroups. In future electrochemical studies, we hope to explore this issue in greater detail.

PM-IRRAS. Surface infrared spectroscopy can provide information regarding the orientation and conformational order of the organic monolayer films.[35,50,51] In our studies, the specific technique of polarization modulation infrared reflection−absorption spectroscopy (PM-IRRAS) was applied. In this technique, the C−H stretching region and especially the frequency and bandwidth of the methylene antisymmetric ($\nu_{as}^{CH_2}$) and symmetric ($\nu_{s}^{CH_2}$) bands are sensitive to the degree of conformational order (crystallinity) of the films.[50−53] For crystalline *n*-docosanethiol, for example, $\nu_{as}^{CH_2}$ and $\nu_{s}^{CH_2}$ appear at 2918 and 2851 cm^{-1}, respectively, while for liquid *n*-docosanethiol, they appear at 2924 and 2855 cm^{-1}, respectively.[35]

Figure 4 shows the C−H stretching region of the infrared spectra for the SAMs generated from **C18** and the new adsorbates. We assigned the bands in Figure 4 on the basis of published data.[51] The $\nu_{as}^{CH_2}$ and $\nu_{s}^{CH_2}$ bands for the SAM derived from **R1ArMT** appear at 2918 and 2851 cm^{-1}, the same as that found for **C18**, indicating a crystalline-like conformational order for both films. The $\nu_{as}^{CH_2}$ bands of **R2ArMT** and **R3ArMT** films broaden and shift to higher frequency at 2923 and 2920 cm^{-1}, respectively. These results indicate that the SAMs derived from the double- and triple-chained adsorbates are less conformationally ordered than those derived from **C18** and **R1ArMT**. As a whole, the IR data suggest the following order for the relative order/crystallinity of the SAMs: **C18** ∼ **R1ArMT** > **R3ArMT** ≫ **R2ArMT**. The data for the SAM derived from **R2ArMT** are particularly striking and indicate a liquidlike conformation for the alkyl chains.

dx.doi.org/10.1021/la201313g |*Langmuir* 2011, 27, 9920–9927

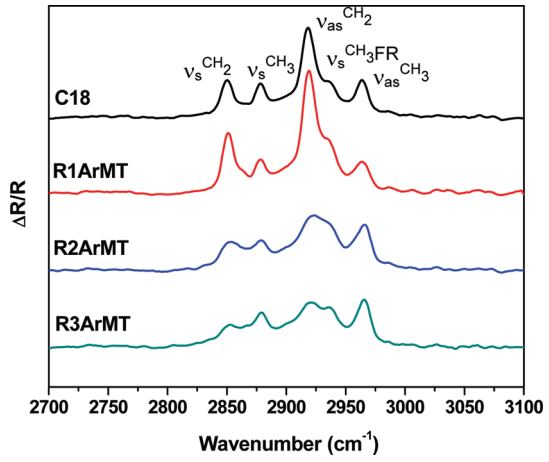

Figure 4. PM-IRRAS spectra of the C−H stretching region for the monolayer films derived from **C18**, **R1ArMT**, **R2ArMT**, and **R3ArMT**.

To discern the interplay of chain packing and orientation induced by the branched chains, further interpretation of the IR spectra is required. The $\nu_s^{CH_3}$ bands of the SAMs generated from **R2ArMT** and **R3ArMT** are more intense than those generated from **C18** and **R1ArMT**, which can be interpreted to indicate that the terminal methyl groups in the **R2ArMT** and **R3ArMT** SAMs are oriented more closely to the surface normal than those in the **C18** and **R1ArMT** SAMs. The broad region from 2890 to 2950 cm^{-1} arises from three overlapping components: the antisymmetric methylene stretching band ($\nu_{as}^{CH_2} \sim 2918-2924$ cm^{-1}), the Fermi resonances (FR) of the symmetric methylene stretching band ($\nu_s^{CH_2}$ FR $\sim$ 2890 cm^{-1}), and the symmetric methyl stretching band ($\nu_s^{CH_3}$ FR $\sim$2935 cm^{-1}).[50,51,54,55] The Fermi resonance bands provide useful information regarding intermolecular interactions and chain assemblies. In the Raman spectra of *n*-alkanes, for example, Snyder et al. reported that the half-width of the $\nu_s^{CH_3}$ FR band is broader in the neat crystal than that in the isolated matrix,[55,56] which suggests that the bandwidth increases with increasing chain−chain interactions and chain packing.[50,51,54] Furthermore, the same phenomenon was observed for the $\nu_s^{CH_2}$ FR band, but the magnitude of the broadening was diminished because of a large difference in frequency between the fundamental and the binary state.[55] Qualitatively, the relative broadness of the Fermi resonances in Figure 4 suggests that chain packing densities are greater in the SAMs derived from **R2ArMT** and **R3ArMT** than in the SAMs derived from **C18** and **R1ArMT**, which is consistent with our interpretation of the XPS data (vide supra).

Another interesting observation is the decrease in the intensity of the bands related to methylene stretching in the **R2ArMT** and **R3ArMT** SAMs compared to the corresponding bands in the **C18** and **R1ArMT** SAMs. On the basis of the surface selection rules for IR spectroscopy, the intensities of both methylene stretching modes decrease with decreasing chain tilt.[14,30,53] Thus, the diminished intensity of the methylene stretching bands might indicate a smaller average tilt angle for the **R2ArMT** and **R3ArMT** SAMs than that in the **C18** and **R1ArMT** SAMs, assuming that all of the monolayers are isotropic and composed of all trans-extended chains. Moreover, a reduced chain tilt (<30°) for the SAMs derived from **R2ArMT** and **R3ArMT** is in good agreement with the ellipsometric thickness data in Table 1, particularly when one considers the almost certainly poor molecular packing underneath the bulky aromatic units of **R2ArMT** and **R3ArMT**. However, despite the trends noted in the IR data here, we caution that changes in frequency, intensity, and bandwidth can arise from a variety of other factors, including chain deformations[35,36] and differences in the twist angles along the axis of the long alkyl chains.[57−59]

Table 3. Advancing (θ_a) and Receding (θ_r) Contact Angles and Hysteresis ($\Delta\theta = \theta_a - \theta_r$) for Hexadecane (HD), Water (H_2O), and Decalin (DEC) on Monolayer Films Generated from C18, R1ArMT, R2ArMT, and R3ArMT

	contact angle (deg)[a]								
	water			hexadecane			decalin		
adsorbate	θ_a	θ_r	$\Delta\theta$	θ_a	θ_r	$\Delta\theta$	θ_a	θ_r	$\Delta\theta$
C18	115	105	10	50	40	10	54	48	6
R1ArMT	115	105	10	50	40	10	54	48	6
R2ArMT	113	103	10	36	30	6	41	34	7
R3ArMT	114	104	10	46	39	7	49	42	7

[a] The average contact angles of water, hexadecane, and decalin were reproducible within ±2°.

To obtain further insight into the structure of the SAMs with regard to the orientation of the aromatic ring, we attempted to examine the low-frequency vibrational data collected by PM-IRRAS in the aromatic C−C stretching and C−H bending region (i.e., 800−1700 cm^{-1}). Despite our efforts, the weak intensity of these modes prohibited any meaningful analysis. We note that previous efforts to analyze the aromatic ring-breathing modes of phenyl-terminated SAMs using our experimental setup were similarly unsuccessful.[9]

Wettabilities of the Films. Contact angle measurements afford wettability data for analyzing interfacial properties and providing insight into the general orientation of the tailgroups of SAMs.[60] Measurements of the advancing and receding contact angles for water, hexadecane, and decalin on the SAMs investigated here are shown in Table 3, where the advancing contact angles for water ($\theta_a^{H_2O}$) are 115°, 115°, 113°, and 114° for the SAMs generated from **C18**, **R1ArMT**, **R2ArMT**, and **R3ArMT**, respectively. These data indicate that the films are similarly hydrophobic.

We also collected contact angle data for hexadecane because this probe liquid is particularly sensitive to small changes in the structure and orientation of hydrocarbon-based films.[14,30,36,61,62] Given, however, that hexadecane can readily intercalate into potential void spaces[20] between the tailgroups in hydrocarbon-based SAMs, we also chose decalin (decahydronapthalene) as a probe liquid because it is less likely to intercalate due to its bulky molecular structure.[22] Table 3 shows that the contact angles for both hexadecane and decalin follow the same trend: **C18** $\sim$ **R1ArMT** > **R3ArMT** $\gg$ **R2ArMT**. The fact that contact angles of water, hexadecane, and decalin are the same for the SAMs derived from **R1ArMT** and **C18** supports our proposal above that the packing and orientation of the **R1ArMT** SAM is similar to that of normal alkanethiolate SAMs. The reduced values for **R3ArMT** and particularly **R2ArMT** are somewhat surprising but can be analyzed by considering both the packing density of the SAMs and the molecular structure of the adsorbates.

Interestingly, the contact angle values of hexadecane (θ_a^{HD}) and decalin (θ_a^{DEC}) drop from their maximum values for the

dx.doi.org/10.1021/la201313g |*Langmuir* 2011, 27, 9920–9927

R3ArMT SAM and drop markedly lower for the **R2ArMT** SAM. This trend is inconsistent with the molecular packing densities measured by XPS, where the relative percent coverages are 100, 81, 68, and 44 for **C18**, **R1ArMT**, **R2ArMT**, and **R3ArMT**, respectively (vide supra). However, the corresponding tailgroup coverages are 100, 81, 136, and 132, respectively, due to the ratio of headgroup:tailgroups for these adsorbates. Given that the contacting liquids probe the tailgroups more than the headgroups of these SAMs, we focus on the tailgroup packing density, orientation, and conformation to interpret the wettability data. As noted above regarding the XPS data, it is likely that the average tilt of the chains in the SAMs is distinct for each adsorbate. Despite this complication, it is still possible to infer structural/conformational information regarding the tailgroups from the PM-IRRAS data. Specifically, the PM-IRRAS data indicate that the conformational order of the tailgroups decreases as follows: **C18** ∼ **R1ArMT** > **R3ArMT** ≫ **R2ArMT**. Importantly, the advancing contact angles of hexadecane and decalin follow the exact same trend (see Table 3). This correlation is consistent with a model in which the tailgroups in the SAMs derived from **R3ArMT** and especially **R2ArMT** are less conformationally ordered (i.e., possess more gauche conformations) and expose a higher fraction of methylene groups at the interface than the SAMs derived from **C18** and **R1ArMT**. As detailed previously, interfacial methylene groups are more wettable than interfacial methyl groups.[62]

Contact angle hysteresis ($\Delta\theta = \theta_a - \theta_r$) can be used to evaluate the relative roughness and/or heterogeneity of surfaces.[63] The hystereses for the SAMs generated from **C18** and the new adsorbates are given in Table 3, which show a constant value of 10° when water is the probe liquid and a constant value of 6°−7° when decalin is the probe liquid. Although the hysteresis values for hexadecane are slightly higher for the **C18** and **R1ArMT** SAMs (10°) than for the **R2ArMT** and **R3ArMT** SAMs (7°), the difference falls within the estimated experimental error. As a whole, the hysteresis data suggest that the chemical and structural homogeneity is largely the same for all of the monolayers.

Proposed Structural Models. To develop an overall picture of how the three adsorbates differ in the formation of monolayer films, we attempted to envision the molecular structures in this system correlated to their molecular orientation and their intramolecular and intermolecular interactions in a thin-film geometry. We first considered an ideal **C18** monolayer film deposited on Au with a $(\sqrt{3} \times \sqrt{3})$R30° lattice structure and a spacing between headgroups of ∼5 Å.[64,65] Because of a slight difference in cross-sectional area between the phenyl ring and the long hydrocarbon chains, the structure of the **R1ArMT** monolayer probably deviates slightly from that in the **C18** monolayer. Introduction of the relatively bulky phenyl ring into the film can plausibly increase the spacing between the chains and thus give rise to a slight increase in the tilt of the chain axis (i.e., >30°). In addition, due to the high degrees of freedom of the C−O bonds in the aromatic adsorbates, the aromatic ring can rotate freely to obtain an optimal orientation (e.g., the molecular plane of the phenyl ring can lie more parallel to the surface normal, maximizing the intermolecular $\pi-\pi$ interactions). Nevertheless, the XPS, PM-IRRAS, and wettability data collectively indicate that the SAM generated by **R1ArMT** is similar to that generated by **C18**, especially with regard to packing density and tailgroup conformation.

For the SAM derived from **R2ArMT**, it is likely that the tailgroups of this adsorbate are aligned roughly normal to the surface (i.e., with little or no tilt at all). This interpretation is supported most strongly by the XPS data, which show that the tailgroups for this adsorbate occupy much less space on the surface of gold (i.e., the footprint of each alkyl chain is markedly smaller) than those of **C18** and **R1ArMT**. Further support is provided by the PM-IRRAS data, which show that the chains in the **R2ArMT** SAM are characterized by liquidlike conformations, and additionally supported by the wettability data, which show markedly lower contact angles for hexadecane and decalin on the liquidlike (i.e., methylene-rich) **R2ArMT** surface. In this model, the **R2ArMT** molecule aligns roughly normal to the surface, and the two pendant alkyl tailgroups are initially splayed by their mutual meta position on the aromatic headgroup. To enhance their van der Waals interactions, the two alkyl chains probably twist toward to each other to maximize the effective chain packing, which leads to a decrease in the average chain tilt and surface area occupied per chain.[66] Given, however, the initial splaying of the chains near the headgroup (and the consequent steric bulk), the chain−chain interactions are apparently insufficient to stabilize a fully trans-extended conformation of the tailgroups. Consequently, this adsorbate generates a film in which the tailgroups are oriented roughly normal to the surface on average and are riddled with gauche conformations that expose a high fraction of methylene groups at the interface.

For the SAM derived from **R3ArMT**, the tailgroups of this adsorbate are probably tilted slightly more than the **R2ArMT** SAM but less than the **C18** and **R1ArMT** SAMs. This interpretation is also supported by the XPS data, which show a slightly lower value of tailgroup packing density than that of **R2ArMT**. The PM-IRRAS and wettability data show, however, that the **R3ArMT** SAM is more conformationally ordered than the **R2ArMT** SAM. Unlike **R2ArMT**, **R3ArMT** has one additional alkyl chain placed at the para position on the aromatic headgroup, which diminishes the void space between two alkyl chains at the ortho positions. We therefore propose a structural model for the **R3ArMT** SAM in which the two alkyl chains at the meta positions twist toward the middle alkyl chain at the para position (see Figure 2). Furthermore, the presence of the middle chain (and the consequent van der Waals stabilization that is concomitant with close molecular packing) appears to alleviate the steric perturbations found in the **R2ArMT** SAM. As such, we propose that the alkyl chains in the **R2ArMT** SAM are tilted no more than 26° from the surface normal on average with a moderate degree of conformational order that exposes mostly methyl groups at the interface.

Unfortunately, precise structural data for these SAMs are difficult to obtain, particularly for the **R2ArMT** and **R3ArMT** SAMs, which lack a high degree of conformational order. Two of the most structurally informative thin-film analyses—diffraction techniques and atomic force microscopy (AFM)—require a high degree of order to obtain lattice parameters.[67] Alternatively, scanning tunneling microscopy (STM) can be used to obtain lattice information, but it is difficult to apply to SAMs that possess long chain lengths.[68]

■ CONCLUSIONS

A series of new adsorbates in which alkoxyphenylethanethiol headgroups having one, two, and three tailgroups were synthesized and used to prepare SAMs on gold. Characterization of these new SAMs showed the following trend in the degree of conformational order in the

monolayer films: **C18** ~ **R1ArMT** > **R3ArMT** > **R2ArMT**. In contrast, the following trend in the relative chain packing densities was observed: **R2ArMT** ~ **R3ArMT** > **C18** > **R1ArMT**. Analysis of the relative molecular and chain packing densities, when coupled with the conformational information provided by PM-IRRAS and wettability measurements, suggests that the alkyl chains for the SAMs derived from **C18** and **R1ArMT** are more highly tilted and occupy more surface area than the alkyl chains of the SAMs derived from **R2ArMT** and **R3ArMT**. As a whole, the results demonstrate the important influence of headgroup:tailgroup ratio on the molecular and chain packing density, tilt angle, conformational order, and the interfacial wettability of organic self-assembled films.

■ ASSOCIATED CONTENT

Supporting Information. Detailed descriptions of the materials and methods used to synthesize the aromatic adsorbates; ^{1}H and ^{13}C NMR spectra of **R1ArMT**, **R2ArMT**, and **R3ArMT**. This material is available free of charge via the Internet at http://pubs.acs.org.

■ AUTHOR INFORMATION

Corresponding Author
*E-mail: trlee@uh.edu.

■ ACKNOWLEDGMENT

We are grateful for generous support from the National Science Foundation (DMR-0906727), the Robert A. Welch Foundation (E-1320), and the Texas Center for Superconductivity at the University of Houston.

■ REFERENCES

(1) Osaka, T. *Chem. Rec.* **2005**, *4*, 346.
(2) Pinnaduwage, L. A.; Gehl, A. C.; Allman, S. L.; Johansson, A.; Boisen, A. *Rev. Sci. Instrum.* **2007**, *78*, 055101/1.
(3) Kim, T.-W.; Wang, G.; Song, H.; Choi, N.-J.; Lee, H.; Lee, T. *J. Nanosci. Nanotechnol.* **2006**, *6*, 3487.
(4) Wyszogrodzka, M.; Haag, R. *Biomacromolecules* **2009**, *10*, 1043.
(5) Andersson, O.; Nikkinen, H.; Kanmert, D.; Enander, K. *Biosens. Bioelectron.* **2009**, *24*, 2458.
(6) Chaki, N. K.; Vijayamohanan, K. *Biosens. Bioelectron.* **2002**, *17*, 1.
(7) Nakano, M.; Ishida, T.; Sano, H.; Sugimura, H.; Miyake, K.; Ando, Y.; Sasaki, S. *Appl. Surf. Sci.* **2008**, *255*, 3040.
(8) Cichomski, M.; Grobelny, J.; Celichowski, G. *Appl. Surf. Sci.* **2008**, *254*, 4273.
(9) Lee, S.; Puck, A.; Graupe, M.; Colorado, R., Jr.; Shon, Y.-S.; Lee, T. R.; Perry, S. S. *Langmuir* **2001**, *17*, 7364.
(10) Carpick, R. W.; Salmeron, M. *Chem. Rev.* **1997**, *97*, 1163.
(11) Arunkumar, P.; Berchmans, S.; Yegnaraman, V. *J. Phys. Chem. C* **2009**, *113*, 8378.
(12) Ulman, A. *Chem. Rev.* **1996**, *96*, 1533.
(13) Love, J. C.; Estroff, L. A.; Kriebel, J. K.; Nuzzo, R. G.; Whitesides, G. M. *Chem. Rev.* **2005**, *105*, 1103.
(14) Laibinis, P. E.; Whitesides, G. M.; Allara, D. L.; Tao, Y. T.; Parikh, A. N.; Nuzzo, R. G. *J. Am. Chem. Soc.* **1991**, *113*, 7152.
(15) Tao, Y. T. *J. Am. Chem. Soc.* **1993**, *115*, 4350.
(16) Tao, Y. T.; Lee, M. T.; Chang, S. C. *J. Am. Chem. Soc.* **1993**, *115*, 9547.
(17) Rieley, H.; Kendall, G. K. *Langmuir* **1999**, *15*, 8867.
(18) Chang, S.-C.; Chao, I.; Tao, Y.-T. *J. Am. Chem. Soc.* **1994**, *116*, 6792.
(19) Sellers, H.; Ulman, A.; Shnidman, Y.; Eilers, J. E. *J. Am. Chem. Soc.* **1993**, *115*, 9389.
(20) Shon, Y.-S.; Colorado, R., Jr.; Williams, C. T.; Bain, C. D.; Lee, T. R. *Langmuir* **2000**, *16*, 541.
(21) Shon, Y.-S.; Lee, T. R. *Langmuir* **1999**, *15*, 1136.
(22) Park, J.-S.; Vo, A. N.; Barriet, D.; Shon, Y.-S.; Lee, T. R. *Langmuir* **2005**, *21*, 2902.
(23) Garg, N.; Lee, T. R. *Langmuir* **1998**, *14*, 3815.
(24) Yu, B.; Qian, L.; Yu, J.; Zhou, Z. *Tribol. Lett.* **2009**, *34*, 1.
(25) Zhang, S.; Jamison, A. C.; Schwartz, D. K.; Lee, T. R. *Langmuir* **2008**, *24*, 10204.
(26) Cimatu, K.; Moore, H. J.; Barriet, D.; Chinwangso, P.; Lee, T. R.; Baldelli, S. *J. Phys. Chem. C* **2008**, *112*, 14529.
(27) Wenzl, I.; Yam, C. M.; Barriet, D.; Lee, T. R. *Langmuir* **2003**, *19*, 10217.
(28) Colorado, R., Jr.; Lee, T. R. *Langmuir* **2003**, *19*, 3288.
(29) Shon, Y.-S.; Kelly, K. F.; Halas, N. J.; Lee, T. R. *Langmuir* **1999**, *15*, 5329.
(30) Nuzzo, R. G.; Dubois, L. H.; Allara, D. L. *J. Am. Chem. Soc.* **1990**, *112*, 558.
(31) Shnidman, Y.; Ulman, A.; Eilers, J. E. *Langmuir* **1993**, *9*, 1071.
(32) Ulman, A.; Scaringe, R. P. *Langmuir* **1992**, *8*, 894.
(33) Evans, S. D.; Urankar, E.; Ulman, A.; Ferris, N. *J. Am. Chem. Soc.* **1991**, *113*, 4121.
(34) Tillman, N.; Ulman, A.; Schildkraut, J. S.; Penner, T. L. *J. Am. Chem. Soc.* **1988**, *110*, 6136.
(35) Porter, M. D.; Bright, T. B.; Allara, D. L.; Chidsey, C. E. D. *J. Am. Chem. Soc.* **1987**, *109*, 3559.
(36) Bain, C. D.; Troughton, E. B.; Tao, Y. T.; Evall, J.; Whitesides, G. M.; Nuzzo, R. G. *J. Am. Chem. Soc.* **1989**, *111*, 321.
(37) Garg, N.; Friedman, J. M.; Lee, T. R. *Langmuir* **2000**, *16*, 4266.
(38) Garg, N.; Carrasquillo-Molina, E.; Lee, T. R. *Langmuir* **2002**, *18*, 2717.
(39) Molecular models were perfromed using the Gaussview03, revision 3.07; Gaussian, Inc., Pittsburgh, PA.
(40) For calculating the theoretical film thicknesses based on the implementation of algorithm only simple geometry and trigonometry, we assumed that the alkyl chains were fully extend and tilted ~ 30° from the surface normal. The following data were used: C−C ~1.5 Å, C−O ~ 1.4 Å, <CCC ~ 109.5°, and <COC ~ 110.8°.
(41) Biebuyck, H. A.; Bain, C. D.; Whitesides, G. M. *Langmuir* **1994**, *10*, 1825.
(42) Ishida, T.; Hara, M.; Kojima, I.; Tsuneda, S.; Nishida, N.; Sasabe, H.; Knoll, W. *Langmuir* **1998**, *14*, 2092.
(43) Yang, Y. W.; Fan, L. J. *Langmuir* **2002**, *18*, 1157.
(44) Castner, D. G.; Hinds, K.; Grainger, D. W. *Langmuir* **1996**, *12*, 5083.
(45) Heeg, J.; Schubert, U.; Kuchenmeister, F. *Fresenius' J. Anal. Chem.* **1999**, *365*, 272.
(46) Park, J.-S.; Smith, A. C.; Lee, T. R. *Langmuir* **2004**, *20*, 5829.
(47) Hallmann, L.; Bashir, A.; Strunskus, T.; Adelung, R.; Staemmler, V.; Woll, C.; Tuczek, F. *Langmuir* **2008**, *24*, 5726.
(48) Himmel, H. J.; Woell, C.; Gerlach, R.; Polanski, G.; Rubahn, H. G. *Langmuir* **1997**, *13*, 602.
(49) Desikan, R.; Armel, S.; Meyer, H. M., III; Thundat, T. *Nanotechnology* **2007**, *18*, 424028/1.
(50) Snyder, R. G.; Strauss, H. L.; Elliger, C. A. *J. Phys. Chem.* **1982**, *86*, 5145.
(51) MacPhail, R. A.; Strauss, H. L.; Snyder, R. G.; Elliger, C. A. *J. Phys. Chem.* **1984**, *88*, 334.
(52) Bensebaa, F.; Ellis, T. H.; Badia, A.; Lennox, R. B. *Langmuir* **1998**, *14*, 2361.
(53) Bensebaa, F.; Ellis, T. H.; Badia, A.; Lennox, R. B. *J. Vac. Sci. Technol., A* **1995**, *13*, 1331.
(54) Snyder, R. G.; Scherer, J. R. *J. Chem. Phys.* **1979**, *71*, 3221.
(55) Snyder, R. G.; Hsu, S. L.; Krimm, S. *Spectrochim. Acta, Part A* **1978**, *34A*, 395.
(56) Hill, I. R.; Levin, I. W. *J. Chem. Phys.* **1979**, *70*, 842.

(57) Parikh, A. N.; Allara, D. L. *J. Chem. Phys.* **1992**, *96*, 927.
(58) Wood, K. A.; Snyder, R. G.; Strauss, H. L. *J. Chem. Phys.* **1989**, *91*, 5255.
(59) Zerbi, G.; Roncone, P.; Longhi, G.; Wunder, S. L. *J. Chem. Phys.* **1988**, *89*, 166.
(60) Whitesides, G. M.; Laibinis, P. E. *Langmuir* **1990**, *6*, 87.
(61) Bain, C. D.; Whitesides, G. M. *Angew. Chem.* **1989**, *101*, 522.
(62) Shon, Y.-S.; Lee, S.; Colorado, R., Jr.; Perry, S. S.; Lee, T. R. *J. Am. Chem. Soc.* **2000**, *122*, 7556.
(63) Johnson, R. E., Jr.; Dettre, R. H. *Surface Colloid Sci.* **1969**, *2*, 85.
(64) Chidsey, C. E. D.; Liu, G. Y.; Rowntree, P.; Scoles, G. *J. Chem. Phys.* **1989**, *91*, 4421.
(65) Strong, L.; Whitesides, G. M. *Langmuir* **1988**, *4*, 546.
(66) Chechik, V.; Schoenherr, H.; Vancso, G. J.; Stirling, C. J. M. *Langmuir* **1998**, *14*, 3003.
(67) Schreiber, F. *Prog. Surf. Sci.* **2000**, *65*, 151.
(68) Poirier, G. E. *Chem. Rev. (Washington, D. C.)* **1997**, *97*, 1117.